UC Davis

UC Davis Previously Published Works

Title

Highly Sensitive and Selective Spiropyran-Based Sensor for Copper(II) Quantification

Permalink

https://escholarship.org/uc/item/3554f2kb

Journal

ACS Omega, 6(16)

ISSN

2470-1343

Authors

Trevino, Kimberly M

Tautges, Brandon K

Kapre, Rohan

et al.

Publication Date

2021-04-27

DOI

10.1021/acsomega.1c00392

Peer reviewed

eScholarship.org Powered by the California Digital Library
University of California

ACS OMEGA

http://pubs.acs.org/journal/acsodf

Article

Highly Sensitive and Selective Spiropyran-Based Sensor for Copper(II) Quantification

Kimberly M. Trevino, Brandon K. Tautges, Rohan Kapre, Francisco C. Franco Jr, Victor W. Or, Edward I. Balmond, Jared T. Shaw, Joel Garcia,* and Angelique Y. Louie*

Cite This: *ACS Omega* 2021, 6, 10776−10789

Read Online

ACCESS | Metrics & More | Article Recommendations | Supporting Information

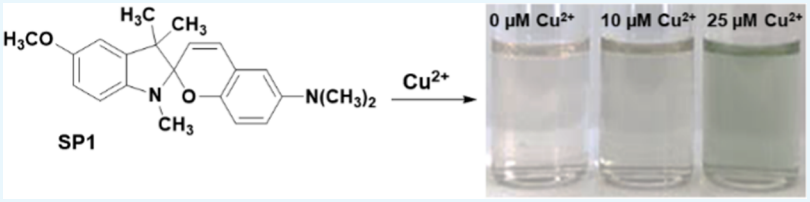

ABSTRACT: The metal-binding capabilities of the spiropyran family of molecular switches have been explored for several purposes from sensing to optical circuits. Metal-selective sensing has been of great interest for applications ranging from environmental assays to industrial quality control, but sensitive metal detection for field-based assays has been elusive. In this work, we demonstrate colorimetric copper sensing at low micromolar levels. Dimethylamine-functionalized spiropyran (**SP1**) was synthesized and its metal-sensing properties were investigated using UV−vis spectrophotometry. The formation of a metal complex between **SP1** and Cu^{2+} was associated with a color change that can be observed by the naked eye as low as ≈6 μM and the limit of detection was found to be 0.11 μM via UV−vis spectrometry. Colorimetric data showed linearity of response in a physiologically relevant range (0−20 μM Cu^{2+}) with high selectivity for Cu^{2+} ions over biologically and environmentally relevant metals such as Na^{+}, K^{+}, Mn^{2+}, Ca^{2+}, Zn^{2+}, Co^{2+}, Mg^{2+}, Ni^{2+}, Fe^{3+}, Cd^{2+}, and Pb^{2+}. Since the color change accompanying **SP1**−Cu^{2+} complex formation could be detected at low micromolar concentrations, **SP1** could be viable for field testing of trace Cu^{2+} ions.

1. INTRODUCTION

Transition metals are essential for many biological functions, including catalysis, metabolism, and signaling.[1,2] The transition metals that are recognized as being critical to biology include iron, zinc, manganese, cobalt, nickel, molybdenum, and copper; physiological imbalances in these metals can lead to several distinct health problems.[3,4] As a cofactor for some 30 enzymes, copper plays an important role in biological processes such catecholamine biosynthesis, ATP production, and protecting the cell from oxygen free radicals.[5,6] Bioavailable copper exists as Cu(I) and Cu(II) in physiological conditions, while Cu(II) is the most stable and is highly redox active, which gives it utility as an antioxidant.[7] However, perturbations in copper(II) homeostasis can be highly toxic to cells and have been linked to the development of neurodegenerative diseases such as Alzheimer's,[8−10] Parkinson's,[11,12] Menkes,[13,14] and amyotrophic lateral sclerosis (ALS).[15,16] In addition to its role in disease, copper(II) can be an undesirable contaminant in soils,[17] water, and even jet fuels.[18] Deleterious effects can occur at low concentrations, for example, aquatic microorganisms can be affected at sub-micromolar concentrations and even trace amounts of copper can accelerate the degradation of fuels.[19−22]

Given the aforementioned significance of copper in biological (aqueous) and industrial (organics) settings, there is keen interest in methods to measure the copper content. Current methods for copper quantification include inductively coupled plasma mass spectrometry (ICP-MS),[23−25] atomic absorption spectroscopy (AAS),[26,27] organic colorimetric sensors,[28−30] and fluorescent sensors.[31,32] Analytical methods such as ICP-MS and AAS offer parts per billion sensitivity, but these methods often require protracted sample extraction, preparation, and the use of sophisticated instruments, precluding use for rapid or in-the-field analysis.[23−27] Fluorescent sensors can provide detection of copper ions without protracted sample preparations but still require advanced instrumentation to analyze the changes in fluorescence.[31,32] Optical, colorimetric sensors for copper offer the potential for naked-eye detection of copper ions without extensive sample manipulation or the use of large instrumentation[28−30] and represent a low-cost, rapid alternative to laboratory testing methods. Furthermore, the development of inexpensive portable UV−vis spectrometry

Received: January 21, 2021
Accepted: April 2, 2021
Published: April 13, 2021

ACS Publications

© 2021 The Authors. Published by American Chemical Society

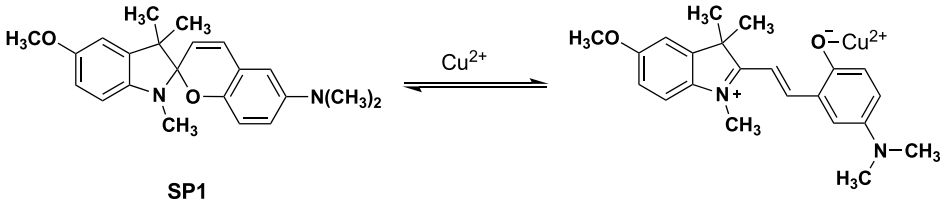

Figure 1. Generalized isomerization of **SP1** in the presence of Cu^{2+}.

Scheme 1. : Synthesis of SP1

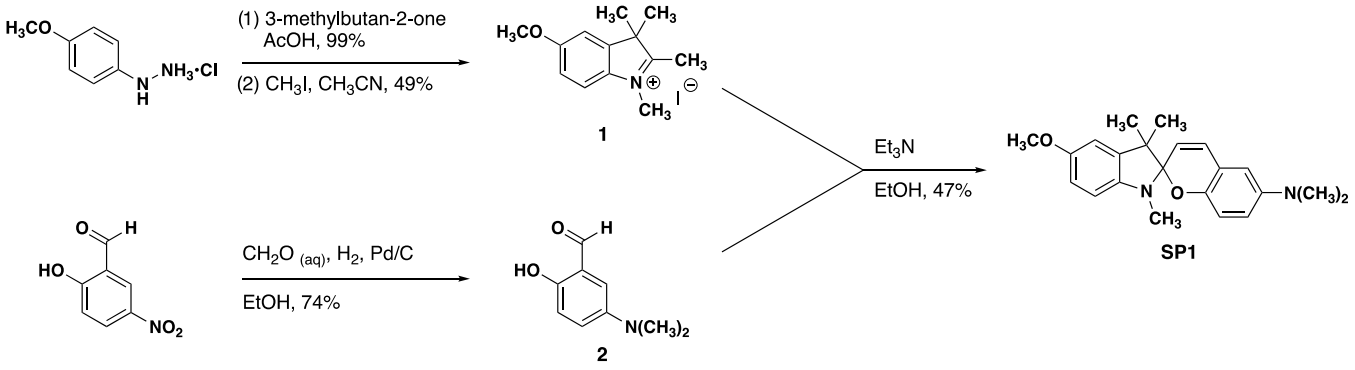

instruments means that highly quantitative sub-micromolar readings could one day be taken directly in the field.[33] This would be particularly useful for the rapid detection and quantification of potentially harmful levels of copper through field testing.

Small-molecule copper-ion sensors that produce optical signals are of great interest and we have identified 55 colorimetric and fluorescent copper sensors that have been reported in the literature in 2010.[28,34−87] Some designs that have been explored include chemosensors based on rhodamine[44,53,56,57,60,78] and Schiff-base units.[28,37,45,48,51,54,61,62,70,71,76,77] It is evident that while there have been many copper sensor designs, sensitivity and selectivity for naked-eye detection remain elusive. For example, of the 55 sensors mentioned above, only 14 sensors displayed naked-eye detection below 10 μM.[34,42,44,50,53,57,61,65,66,69,70,72,76,87] Furthermore, only three of the studies challenged copper sensing in the presence of a competing metal ion[34,61,70] and none challenged copper sensing in the presence of 10-fold excess competing metal to copper, which is achieved in this work.

Spiropyrans and their derivatives have been utilized for the detection of copper(II) ions[80−87] However, most of these sensors suffer from low sensitivity for naked-eye detection with the concentration of Cu^{2+} detection ranging primarily from 20 μM to 2 mM,[80−86] which can be above critical thresholds of interest, such as in environmental contamination. Of the spiropyran-based copper sensors previously referenced, only one demonstrated naked-eye detection below 10 μM for the spiropyran−copper(II) complex.[87] This spironaphthanopyran that was able to detect copper(II) concentrations as low as 1 μM by the naked eye. The isomerization of spiropyran to merocyanine establishes the thermo-/photostable isomer due to the intramolecular hydrogen bonding between the naphthanolate and the adjacent hydroxyl group. The color change is inconsistent, going from pinkish-violet in the absence of copper to violet at 1 μM and to blue at 10 μM. The distinct color change from purple to blue is proposed to be due to copper(II) metal ligation to the naphthanolate and the hydroxyl group; it appears to bind in 2:1 stoichiometry of sensor/copper. Competitive binding experiments were performed with the sensor (10 μM) to Cu^{2+} (10 μM), mixed with other metal ions (50 μM) via a UV−vis spectrometer; however, naked-eye detection under these conditions was not reported. In addition, mechanistic studies were not performed.

In this work, we report a dimethylamine-functionalized spiropyran, **SP1**, sensor for copper(II) with naked-eye detection down to ≈6 μM and a limit of detection (LOD) of 0.11 μM, showing promise for in-the-field applications. We have found that placing an electron-donating group on the indoline portion of a spiropyran yielded an enhanced metal-ion response for optical detection.[88] With this information, we developed a methoxy-functionalized spiropyran with pendant dimethylamine on the chromene portion in an effort to enhance sensitivity while maintaining high copper(II) selectivity (Figure 1). We have previously reported the synthesis of this spiropyran derivative.[88] Herein, we examine the metal sensitivity and selectivity of this derivative for copper(II) ions.

2. RESULTS AND DISCUSSION

The synthesis of **SP1** proceeded conveniently through the convergent synthesis of the appropriate indolium iodide and dimethylaminobenzaldehyde (Scheme 1). The indolium iodide was prepared from the methoxyhydrazine through an interrupted Fisher indole synthesis, followed by methylation with iodomethane. The one-pot reduction and methylation of 2-hydroxy-5-nitrobenzaldehyde with palladium on carbon, formaldehyde, and hydrogen afforded the requisite 5-dimethylamino-2-hydroxybenzaldehyde. Subsequent condensation of the indolium iodide with 5-dimethylamino-2-hydroxybenzaldehyde, in the presence of Et_3N, afforded **SP1**.

In an effort to evaluate the relative photochromism of **SP1**, the absorption profile was compared before and after irradiation with UV light. Figure 2A shows the absorption

https://doi.org/10.1021/acsomega.1c00392
ACS Omega 2021, 6, 10776−10789

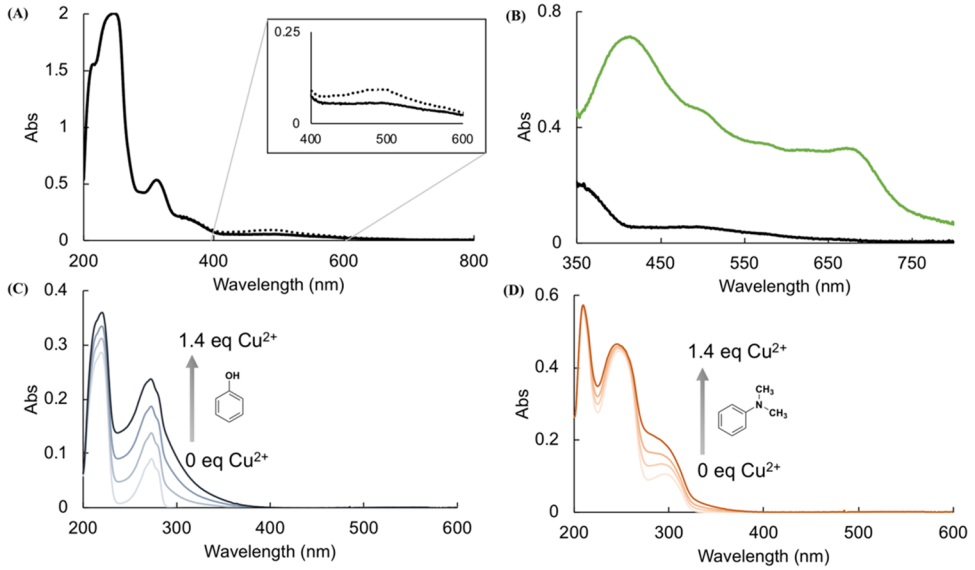

Figure 2. (A) Absorbance profile of **SP1** (100 μM in ethanol) after preparation in the dark (black, solid) and after 15 min UV irradiation at 302 nm with an 8 W UV source (black, dotted). The inset shows the modest increase (0.04 AU) in response to UV irradiation, indicating minor photoswitching for **SP1**. (B) Absorbance profile of **SP1** in the absence (black) and the presence (green) of Cu^{2+}. Response of reference compounds (100 μM): (C) phenol and (D) *N*,*N*-dimethylaniline to varying amounts (0−1.4 equiv) of Cu^{2+} in ethanol.

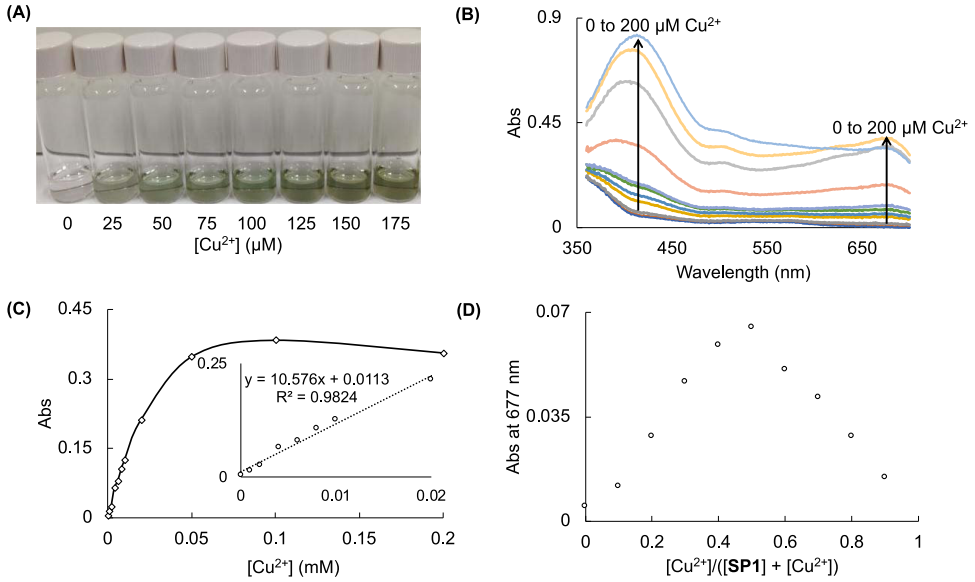

Figure 3. (A) Color change observed for **SP1** with increasing concentrations of copper(II). An observable change in the color between concentrations suggests that **SP1** is capable of being used in the field for naked-eye qualitative assessment of the copper(II) concentration. (B) Absorbance profile of **SP1** incubated with various concentrations of Cu^{2+}: 1 μM (orange); 2 μM (gray); 4 μM (gold); 6 μM (blue); 8 μM (green); 10 μM (light blue); 25 μM (light orange); 50 μM (light gray); 100 μM (yellow); and 200 μM (blue). (C) **SP1** titrated with various concentrations of copper(II) with the absorbance measured at 677 nm. This titration study demonstrates a nearly linear response through 20 μM Cu^{2+}, indicating the utility of **SP1** as a quantitative sensor for copper through 50 μM concentrations of copper(II). The inset shows the linearity of response from 0 to 20 μM. (D) Job's analysis of the **SP1**−Cu^{2+} complex in ethanol. Absorbance recorded at 677 nm with maximal absorbance achieved at a 0.5 molar fraction of copper(II), indicating a stoichiometry of 1:1 for the **SP1**−Cu^{2+} complex.

spectral changes of **SP1** after UV irradiation. Prior to UV exposure, the absorption plot of **SP1** is characterized by large absorbance bands at 250 and 312 nm, corresponding to the ring-closed spiro (SP) form (Figure 2A, solid line). No significant absorption was found in the visible region, which suggests that most of **SP1** was present in its spiro form. It was postulated that the electron-donating character of the amine substituent on chromene suppresses spiro-to-mero conversion.[82] Upon irradiation with UV light, a modest increase in absorbance (0.04 AU) at 483 nm, corresponding to the ring-open mero (MC) form, was observed (Figure 2A, dotted line). While the UV−vis spectrum suggested that the absorption properties of **SP1** were minimally influenced by UV light, addition of 1 equiv of Cu^{2+} to a solution of **SP1** in ethanol with a 15 min incubation period produced a green solution with strong mero absorption bands centered at 418 and 677 nm. A hypsochromic shift of the mero lambda max from 483 to 418 nm (Figure 2B) was observed, which could be attributed to the

https://doi.org/10.1021/acsomega.1c00392
ACS Omega 2021, 6, 10776−10789

change in the local environment such as an increase in the ionic strength due to the added copper(II) salt in the solution. The strong absorption band at 677 nm was assigned to possible **SP1**−Cu^{2+} complex in solution; this bathochromic shift of the mero band from 483 to 677 nm was consistent with reported absorbance changes accompanying the formation of the MC−Cu^{2+} complex exhibited by quinaldine-indole-based spiropyran.[86] Copper(II) is an intermediate hard Lewis acid and therefore is hypothesized to preferentially interact with hard Lewis bases such as dimethylamino and phenolic oxygen groups on chromene, forming MC−Cu^{2+} adducts.

To test the hypothesis of copper(II) binding to phenolic and/or dimethylamine groups on chromene, we investigated the changes in the UV−vis profile of the reference compounds: phenol and *N*,*N*-dimethylaniline upon addition of copper(II) in ethanol (Figure 2C,D). In the presence of copper(II), significant increases in absorbance were observed in the 250−375 nm range for both molecules. The absorbance in this wavelength range continually increased as more copper(II) ions were introduced. These copper(II)-induced changes in UV−vis profile indicate that the methylated amine and phenolic oxygen in **SP1** are capable of interacting with copper(II). Theoretical calculations of copper interactions with **SP1** yielded several minima including binding of copper to the phenolic oxygen or the dimethylamine, where binding to phenolic oxygen was the lowest energy and most stable option (Figure S6). This binding is illustrated in Figure 1. Also, this UV−vis data underscore the importance of the amine substituent for copper(II) sensing as the electron-donating character of the former is expected to stabilize the spiro form of **SP1**, forming a photostationary spiropyran state.[89] Upon coordinately binding to copper(II) ion, the electron-donating character of the methylated amine decreases, consequently favoring spiro-to-mero conversion, as illustrated by the appearance of strong mero bands in the visible region in Figure 2B.

The sensitivity of **SP1** for a copper(II) ion was evaluated by colorimetric and titration studies with concentrations of copper(II) varying from 0 to 200 μM. The distinct visual color change of **SP1** allows qualitative differentiation among different concentrations of copper(II) ions present (Figure 3A). In the absence of copper(II), the solution of **SP1** is light pink in color; however, after incubating with 25 μM copper(II) for 15 min, the color of the **SP1** solution changed to green. This green color became progressively darker as the copper(II) concentration was increased from 25 to 175 μM copper(II), which could allow a field user to employ **SP1** much like a pH strip to roughly quantify the copper(II) concentration. To validate this concentration-dependent darkening of the green color, the absorption profile of **SP1** was monitored as aliquots of copper(II) chloride were added to the solution of **SP1**. A significant increase in the absorbance of **SP1** at 418 and 677 nm was evident with increasing concentration of the copper(II) ion (Figure 3B).

To resolve that copper(II) chloride alone was not inducing the green color, concentrations ranging from 0 to 175 μM copper(II) chloride in ethanol were evaluated (Figure S8). No visual color was observed for copper(II) chloride at these concentrations. In addition, the absorbance profile of copper(II) chloride displayed no absorbance peaks at 418 or 677 nm, further indicating that the **SP1**−Cu^{2+} interaction prompts the color change. The linearity of **SP1** and copper(II) interaction was also assessed and it was found that the absorbance increase was linear from 0 to 20 μM copper(II) (inset, Figure 3C) with no increase in absorbance seen at 677 nm after 1 equiv of copper(II) had been surpassed, suggesting possible 1:1 copper(II)−ligand stoichiometry (Figure 3C). The 1:1 stoichiometry paired with the observations above for binding of copper(II) to reference compounds bearing either amine or phenolic oxygen moieties rules out the possibility of two different copper(II) ions binding simultaneously to dimethylamine *N* and phenolic *O*.

The stoichiometry of **SP1** and copper(II) was validated by Job's method; it is a widely used analytical technique to determine the stoichiometry of a binding event. This method keeps the total molar concentration of two binding components constant while varying the molar fraction of one binding component. In this study, the molar fraction of copper(II) was varied from 0 to 0.9 while keeping the sum of the initial concentration of **SP1** and the copper(II) ion at 100 μM. The absorbance for each molar fraction of copper(II) was recorded at 677 nm and was plotted against the molar fraction of the copper(II) ion, as shown in Figure 3D. The maximum absorbance was achieved at a molar fraction of 0.5, indicating a 1:1 stoichiometry of the **SP1** and the copper(II) ion. This stoichiometry is consistent with previous spiropyran-based colorimetric metal sensors, which often exhibited a 2:1 or 1:1 ligand−copper(II) stoichiometry.[89,90]

To determine the limit of detection (LOD) for copper(II) detection using **SP1**, the change in absorption was plotted against the [Cu^{2+}] concentration. The detection limit of 0.11 μM by means of UV−vis spectrometry was determined by calculating the [Cu^{2+}] at 3SD (SD estimated using the root-mean-square error (MSE) of 0.0022) above the estimated intercept (0.0070) of the linear regression (Figure 4A).

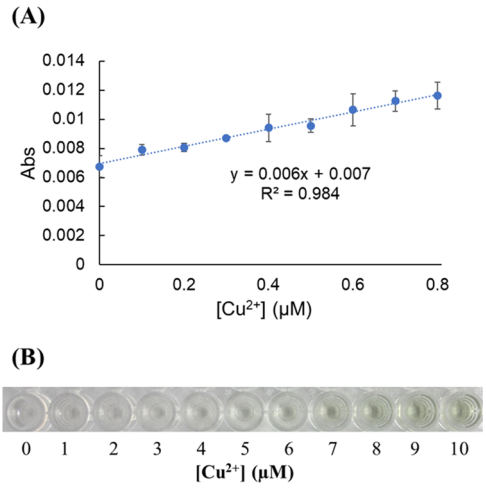

Figure 4. (A) LOD curve for **SP1** incubated with copper (II) concentrations ranging from 0 to 0.8 μM. The LOD was found to be 0.11 μM. (B) Naked-eye detection of **SP1** incubated with increasing concentrations of copper(II) chloride, depicts visual identification of copper(II) ≈ 6 μM.

Compared to other spiropyran-based colorimetric copper(II) sensors, **SP1** exhibited the second-lowest limit of detection relative to other spiropyran-based colorimetric copper(II) sensors previously mentioned.[80−87,91] It is interesting to note the minor structural variations that contribute to the varying limits of detection. Amine placement and other electron-donating groups on the indole may provide greater enhance-

https://doi.org/10.1021/acsomega.1c00392
ACS Omega 2021, 6, 10776−10789

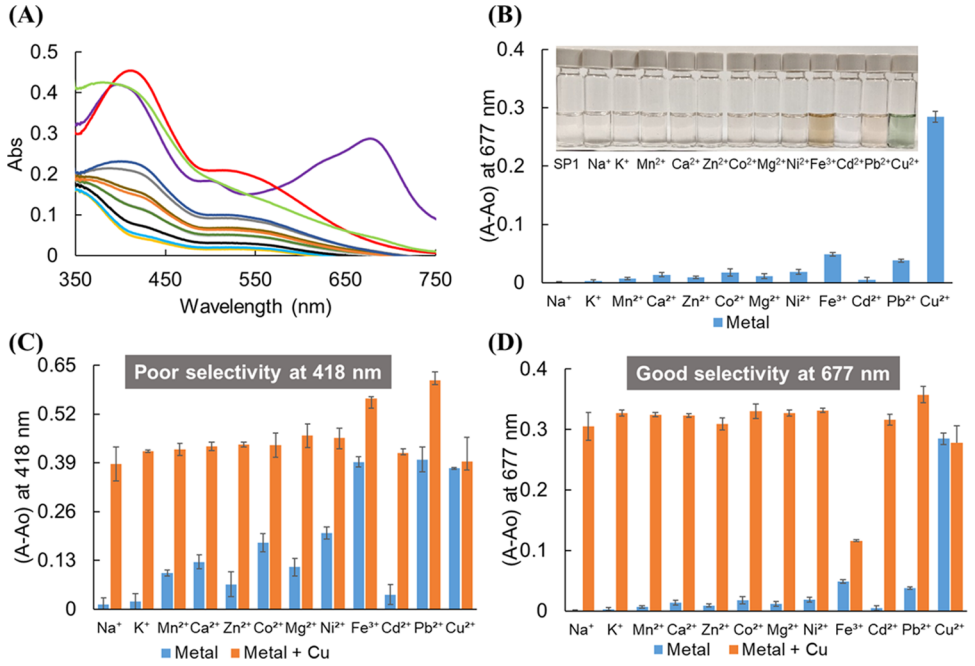

Figure 5. (A) Absorbance profile of **SP1** after 15 min incubation with 1 equiv of various metal chlorides: Cu^{2+} (purple), Fe^{3+} (red), Ni^{2+} (dark blue), Mg^{2+} (orange), Co^{2+} (gray), Zn^{2+} (green), Ca^{2+} (brown), Mn^{2+} (light gray), K^{+} (light blue), Na^{+} (yellow), Cd^{2+} (black), and Pb^{2+} (light green). (B) Relative absorbance increases at 677 nm of **SP1** incubated for 15 min with 1 equiv of various metals. Blue bars represent the change in the absorbance versus initial absorbance to give the relative absorbance increases at 677 nm (inset: naked-eye detection of Cu^{2+} and other metals using **SP1**). (C) Competitive binding experiment with 1 equiv of copper(II) in the presence of 1 equiv of competing metal ions monitored at (C) 418 nm and (D) 677 nm. Blue bars represent the change in the absorbance when **SP1** is incubated with 1 equiv of only one metal ion. Orange bars represent the change in the absorbance for **SP1** when incubated with 1 equiv copper(II) and 1 equiv of a competing metal ion. The orange bars demonstrate that the response of **SP1** to copper(II) is unaffected by the presence of competing metals. These results verify that **SP1** can be used to detect copper(II) reliably regardless of the other metal ions present in the solution. Error bars represent standard deviation of three trials.

ment of this observed sensitivity and will be the focus of future studies.

The sensitivity of **SP1** was further investigated at micromolar levels (0−10 μM Cu^{2+} in deionized ultrafiltered (D.I.U.F) water) by subsequently varying the copper(II) concentration to a solution of **SP1** and monitoring the color change over a 15 min period. Figure 4B illustrates that, through naked-eye detection, **SP1** permits discrimination of ≈6 μM copper(II) concentration over the control and can accurately quantify micromolar concentrations of copper(II). These results support the use of **SP1** at concentrations well below physiological copper(II) ion concentrations (16 μM in serum, 300 μM in cells).[92]

Because of the promising sensitivity of **SP1** toward copper(II), we also studied selectivity by monitoring the changes in the UV−visible absorption profile of **SP1** in response to chloride salts of other biologically and environmentally relevant metals such as Na^{+}, K^{+}, Mn^{2+}, Ca^{2+}, Zn^{2+}, Co^{2+}, Mg^{2+}, Ni^{2+}, Fe^{3+}, Cd^{2+}, and Pb^{2+} in equimolar concentration. Selectivity of some sensors toward copper(II) over other metal ions has been attributed to the strong affinity of the copper(II) ion toward *N*,*O*-chelated ligands and the fast metal-to-ligand binding kinetics of copper(II) to its ligand.[89] Thus, we hypothesize that the presence of the amine substituent in our **SP1** ligand could provide copper(II) selectivity over possible confounding alkali, alkaline-earth, and transition-metal ions. To test this hypothesis, the absorption spectra of **SP1** were taken after incubation with 1 equiv of each metal salt (metal stock in D.I.U.F water). The presence of the distinct absorbance band at 677 nm allowed for copper(II) quantification over the other metal ions tested, which exhibited that absorbance increases only at 418 nm when incubated with **SP1** in ethanol (Figure 5A, copper = purple line). Metal-ion selectivity was also quantified based on the relative absorbance increase of **SP1** at 677 nm when incubated with 1 equiv of various metals (Figure 5B). Absorbance data showed **SP1** exhibiting a nearly 21-fold increase over the baseline when incubated with copper(II), which is almost sixfold greater change in the absorbance at 677 nm compared to the next best metal ion, Fe^{3+} ($p < 0.0010$, Welch's 2 sample *t*-test). Interestingly, copper is the only metal tested to exhibit a green solution with **SP1**; other metals produced pink to reddish-brown color (Figure 5B, inset).

The binding specificity of **SP1** for copper(II) was further characterized by competition studies where the absorbance of **SP1** with 1 equiv of a competitive metal ion was determined in the presence and the absence of 1 equiv of Cu^{2+} at 418 and 677 nm. At 418 nm, other metal ions such as Mn^{2+}, Ca^{2+}, Zn^{2+}, Co^{2+}, Mg^{2+}, Ni^{2+}, Pb^{2+}, and Fe^{3+} induced significant absorbance changes (Figure 5A,C), and therefore could confound analysis of copper(II) levels if measurements were done at this wavelength; thus, the sensor should not be used at 418 nm. In contrast, Figure 5A,D shows that when absorbance was monitored at 677 nm, there was no absorbance at 677 nm for other metals except iron and lead, which showed much lower absorbance than copper. Therefore, 677 nm is recommended for copper sensing. However, there is a diminished response to copper(II) when iron(III) is present, suggesting that iron may interfere with Cu detection. The absorbance profile for each metal chloride at 1×10^{-4} M in

https://doi.org/10.1021/acsomega.1c00392
ACS Omega 2021, 6, 10776−10789

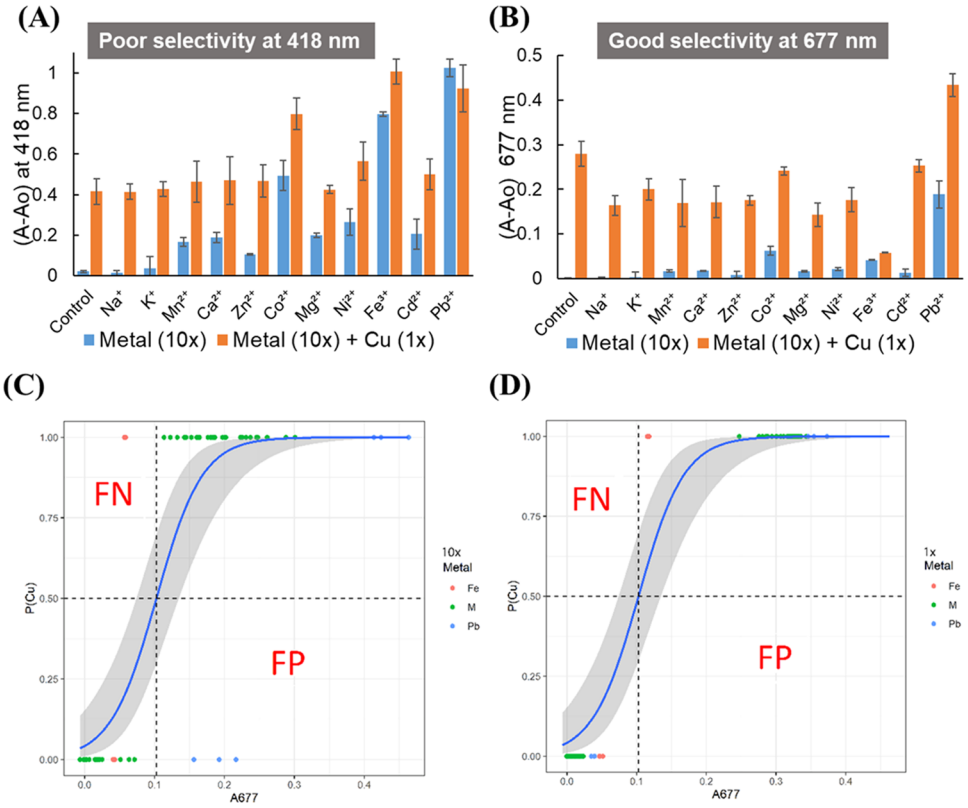

Figure 6. Competitive binding experiment of **SP1** with 1 equiv of copper(II) chloride in the presence of 10 equiv of competing metal ions monitored at (A) 418 nm and (B) 677 nm. Blue bars represent the change in the absorbance when **SP1** is incubated with 10 equiv of only one metal ion. Orange bars represent the change in the absorbance for **SP1** when incubated with 10 equiv of a competing metal ion and 1 equiv of copper(II) chloride. **SP1** incubated without (blue) and with (orange) 1 equiv of copper(II) was used as the control. (C) Logistic regression fitted on 10× data. The only errors (as assessed by leave-one-out cross-validation) occur for false positive (FP) and false negative (FN) occur for Pb and Fe, respectively. The cutoff for absorbance at 0.5 probability of Cu was 0.103. The gray region represents 95% confidence interval (CI). (D) 10× logistic regression fit overlayed on 1× data. When used to predict the presence of Cu under 1× of other metals, no FP or FN occur on this data set.

ethanol was also evaluated (Figure S9). Metal ions Fe^{3+} and Pb^{2+} contained some absorbance at 418 nm, which could explain the relatively higher absorbance compared to the other metal ions with and without Cu^{2+}. None of the other metal ions displayed an absorbance at 677 nm. These results indicate that quantitative, relatively specific determination of Cu^{2+} levels using **SP1** would be possible if measurements are done at 677 nm. This wavelength-dependent copper(II) selectivity by **SP1** could be particularly useful, for example, when samples contain a high concentration of other ions such as Mn^{2+} and K^{+}, two of the common ions found in soil.

To further test the detection capability of **SP1** for copper(II), the competition study was repeated at higher concentrations of competing metal, and the absorbance of **SP1** was evaluated at 418 and 677 nm with 10 equiv of a competitive metal ion in the presence and the absence of 1 equiv of Cu^{2+} (Figure 6). **SP1** incubated with and without 1 equiv of copper(II) was used as the control. Analysis done at 418 nm with **SP1** in the presence of 10 equiv of the metal displayed that all ions except Na^{+} and K^{+} induced an increase in the absorbance at that wavelength (Figure 6A). When 1 equiv of Cu^{2+} was added, it is noted there was an additional increase in absorbance for each metal ion at 418 nm except Pb^{2+}. Due to the significant absorbances of metal ions, such as Mn^{2+}, Ca^{2+}, Zn^{2+}, Mg^{2+}, Ni^{2+}, Cd^{2+}, Co^{2+}, Fe^{3+}, and Pb^{2+}, as previously noted, analysis at this wavelength would confound copper(II) detection. Therefore, 677 nm was again inspected (Figure 6B). At 677 nm, metal ions Co^{2+}, Fe^{3+}, and Pb^{2+} exhibited some absorbance. However, when incubated with SP alone, both Co^{2+} and Pb^{2+} did not display the bathochromic shift associated with the SP−Cu^{2+} complex (Figure S11.A). Only in the presence of one added equivalent of copper(II), the strong absorbance band at 677 nm is witnessed (Figure S11.B). Copper can again be detected by eye through a notable change to a greenish solution with the addition of 1 equiv of copper, even in the presence of 10× excess competing metals, with the exception of Fe^{3+} and Pb^{2+} (Figure S11.D). As for the 1:1 studies, monitoring the sensor at 677 nm provided optimal selectivity for copper, As expected with Fe^{3+}, there was a diminished response to copper(II), which was previously seen in the equimolar competition studies. At 10× excess, lead also contributes absorption that confounds copper interpretation, but it should be noted that the levels of lead represented by 10× are very high on the order of lead concentrations in water found during the height of the Flint Michigan crisis.[93] There are several feasible approaches to navigate around these interferences. For example, the establishment of pretreatment methods, such as a Fe^{3+} chelator that could effectively remove this metal ion from the sample. Singha et al. developed rhodamine-functionalized mesoporous silica to remove Fe^{3+} from solutions.[94] Due to the mesoporous solid support, this material can be effectively removed via filtration. Lead is a contaminant of great health concern and a number of separate sensors for lead have been developed,[95] which could be used to

https://doi.org/10.1021/acsomega.1c00392
ACS Omega 2021, 6, 10776−10789

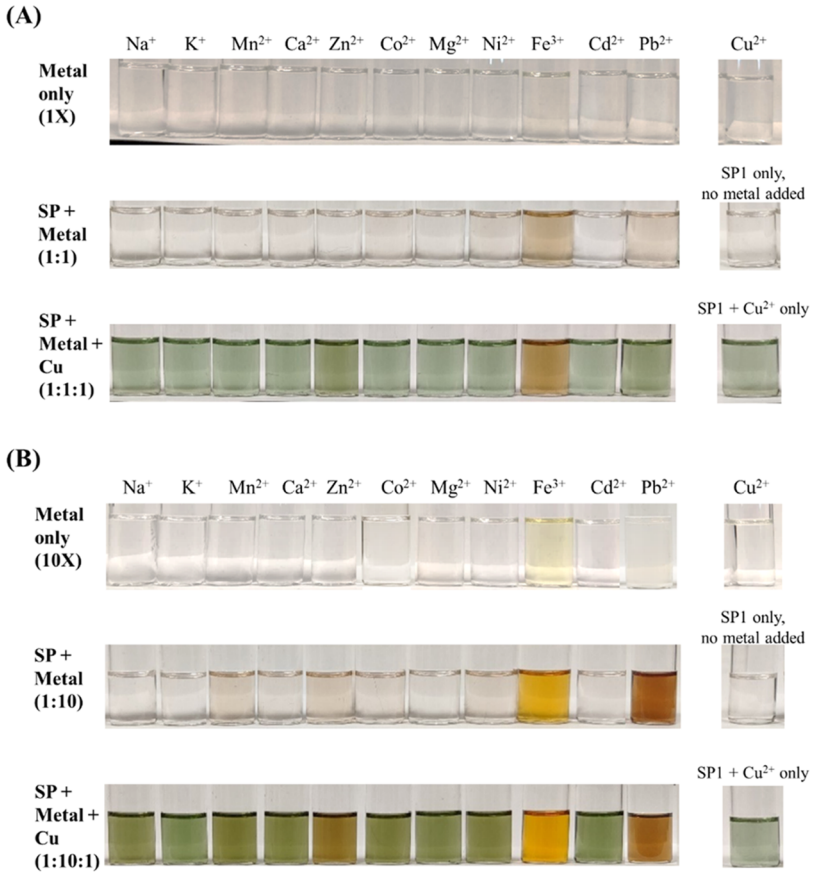

Figure 7. Summary of naked-eye, colorimetric, selective detection of copper(II) by **SP1**. Samples are shown in the presence and the absence of (A) 1× and (B) 10× competing metals.

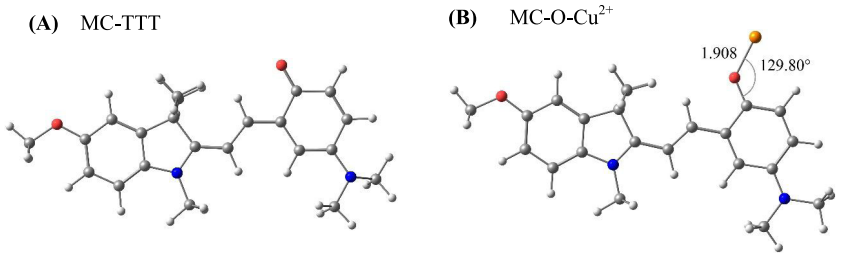

Figure 8. DFT calculations were used to determine the (A) TTT isomer to be the most stable ring-open mero form and the (B) phenolic oxygen to be the strongest interaction between **SP1** and Cu^{2+} (orange).

identify lead vs copper contribution. Furthermore, copper still confers a distinct green color even in the presence of 10× competing metals (Figure S11.D), for all metals except iron and lead, both of which are also undesirable contaminants; a field test with **SP1** could be used as an initial screening mechanism to determine if samples contain any of these three undesirable metals and need to be brought back for further lab analysis by other more sensitive methods.

The logistic regression model depicted in Figure 6C,D demonstrates the type of field test that could be used. We found that the logistic regression model on the 10× data (n = 72) has an overall accuracy of $\frac{66+1}{72+2}$ = 90.54%, as calculated through leave-one-out cross-validation followed by the adjustment via Laplace's rule.[96] The errors are 3/3 false negatives (FN) for Fe and 3/3 false positives (FP) for Pb. However, when this same model is trained on the 10× data is used to predict the 1× data (n = 72), the overall accuracy is approximately $\frac{72+1}{72+2}$ = 98.65% after adjustment via Laplace's rule. No false positives or false negatives are seen for any metal with the 10× logistic regression used to predict Cu in the 1× data set. The cutoff found for absorbance at 677 nm for 50% probability of Cu was 0.103. This further suggests that the **SP1** sensor is adequate as an initial field test.

The naked-eye, colorimetric, selective detection of copper by **SP1** is summarized and presented in Figure 7A for 1× competing metals and Figure 7B for 10× competing metals. These photographs mirror the solutions from the absorbance spectrophotometry studies previously discussed. As shown in Figure 7A, the 1× metals alone do not impart color to the solution. **SP1** with metals at 1× plus are colorless to pink, except for copper(II), which is green. When copper is introduced to **SP1** in the presence of a 1:1 equivalent competing ion, Cu^{2+}, this solution is still green, except for Fe^{3+}, which is brownish-green. Figure 7B reveals that metals alone at

https://doi.org/10.1021/acsomega.1c00392
ACS Omega 2021, 6, 10776−10789

10× do not possess any significant color, except for iron, which is light yellow. When the **SP1** sensor is present in the 10× metal solution, all are colorless to light pink except for Fe^{3+} and Pb^{2+}. **SP1** plus copper in the presence of 10:1 molar equivalent competing metal, Cu^{2+}, maintains the green color, except for Fe^{3+}, which is yellow, and Pb^{2+}, which is brown. These results demonstrate the ability of **SP1** to detect copper even in the presence of excess amounts of other potential contaminating metals.

Theoretical calculations were carried out to understand the electronic structure of the **SP1**−Cu^{2+} complex and the interaction between spiropyran and copper(II). Density functional theory (DFT) calculations were carried out using the Gaussian16[97] package. The ring-open mero form of **SP1** may assume several conformations (CTC, TTC, TTT, and CTT, where C = cis and T = trans) via the rotation of the three bonds linking the indole and phenolic units. The ring-open mero isomers of **SP1** were observed to have planar structure, while the closed form has the indole and benzopyran groups almost perpendicular to each other. Determination of the energies of the stereoisomers revealed that the TTT isomer is the most stable isomer (Figure 8A). The second-lowest TTC isomer is only 0.57 kJ/mol higher than TTT.

The structure of the complex between **SP1** (TTT) and Cu^{2+} was then determined by placing the Cu^{2+} around the **SP1** molecule. Several minima were observed, and the strongest interaction was seen when Cu^{2+} interacts with O of the phenolic group (Figure 8B). This is due to the negative charge on the O atom (Q_{NBO} = −0.723 e^-) and the positive charge on the Cu (Q_{Cu} = +0.946 e^-), resulting in strong electrostatic interaction (Table S1).

The frontier molecular orbitals (FMOs) of the closed form, open-form, and the **SP1**−Cu^{2+} complex are shown in Figure 9.

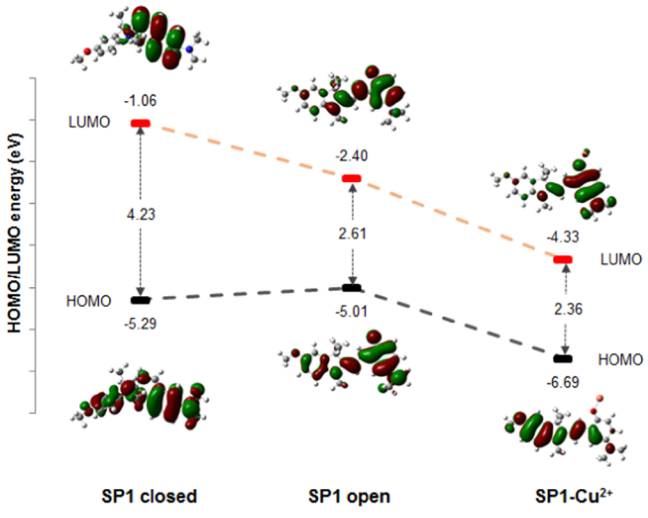

Figure 9. HOMO and LUMO orbitals and energy levels of closed form, open form, and the **SP1**−Cu^{2+} complex.

The highest occupied molecular orbital (HOMO) orbital in the closed form is delocalized in the whole molecule, while the lowest occupied molecular orbital (LUMO) orbital is localized in the benzopyran group. For the open form, both the HOMO and LUMO orbitals are delocalized in the whole molecule. In the **SP1**−Cu^{2+} complex, the HOMO orbital is localized mainly in the indoline group (donor), while the LUMO orbital is localized in the phenol group including the Cu^{2+} ion (acceptor). The HOMO energy from the closed form (−5.29 eV) to the open form (−5.01 eV) increased, while the LUMO energy from the closed form (−1.06 eV) to the open form (−2.40 eV) decreased. These changes resulted in the lowering of the energy gap, E_{Gap}, (4.23−2.61 eV) due to the increase in the conjugation[98] of **SP1**, consistent with the results shown in Figure 2A. Upon binding with Cu^{2+}, both the HOMO (−6.69 eV) and LUMO (−4.33 eV) energies decreased, with the LUMO energy decreased more than the HOMO energy (Table S1). The decrease in the HOMO/LUMO orbitals for the **SP1**−Cu^{2+} is due to the significantly low HOMO (−17.28 eV) and LUMO (−11.07 eV) energies of Cu^{2+}, thus Cu^{2+} accepts electron charge from the **SP1** molecule, resulting in a net increase in the charge of Cu^{2+}, i.e., from +2 e^- for isolated Cu^{2+} to +0.946 e^- (Q_{NBO}) in the **SP1**−Cu^{2+} complex. This resulted in the lowering of E_{Gap}, consistent with the bathochromic shift observed in Figure 2B and UV−vis simulation (Figure S7). We also determined the HOMO−LUMO gaps (Figure S16) of several **SP1**−metal complexes and observed that the energy gap of **SP1**−Cu^{2+} is significantly smaller compared to the other **SP1**−metal complexes and could explain why the **SP1**−Cu^{2+} complex absorbs at a longer wavelength than the other SP1−metal complexes.

3. CONCLUSIONS

In this work, we demonstrated the metal selectivity and sensing properties of a spiropyran molecular sensor. **SP1** showed selectivity toward copper(II) ions, which offered qualitative naked-eye detection (colorless to green) and quantitative detection of copper(II). The sensor demonstrated two absorbance maxima in response to metal ions with selectivity for copper(II) at a wavelength of 677 nm. The stoichiometry of metal binding was determined to be 1:1 and was consistent with other copper(II) colorimetric sensors.[81,89] Detection was possible even in the presence of 10× molar equivalents of other metals, with exception of iron and lead. **SP1** exhibited sensitivity down to the micromolar range with a calculated limit of detection of 0.11 × 10^{-6} M. In addition, the ability to visually detect copper(II) concentrations down to ≈6 μM offers the potential for sensitive and rapid sensing in field samples.

We acknowledge that sensing in a solvent such as ethanol has some limitations; however, contaminants in organics can also be an issue and this system could be useful for other applications such as copper sensing in jet fuels, which is hampered by the volatility during typical analysis techniques.[18] The use of organics to enhance sensor solubility is not unusual. Of the 14 sensors with sub 10 μM sensitivity, similar to ours, 12 of these were in pure solvent or mixtures of solvents such as acetonitrile, methanol, dimethyl sulfoxide (DMSO), or ethanol. Two papers report results in water, but neither of these papers demonstrates naked-eye detection even in the presence of competing metals. While **SP1** has limited solubility in water, efforts are currently underway to apply this sensor in paper-based diagnostics, and preliminary evidence shows that the sensor dried to paper can sense solutions of copper in water. We are also working to adapt this system for 100% aqueous applications by increasing solubility. Although it is a concern that spiropyrans undergo spontaneous ring opening in water, there have been studies in which spiropyrans revealed to be an effective probe in phosphate-buffered saline (PBS)[87] and water.[99] As presented here, copper can be detected by visual

https://doi.org/10.1021/acsomega.1c00392
ACS Omega 2021, 6, 10776−10789

inspection at low concentrations under a number of conditions, which could provide first-pass analysis of the copper content in the field. Further experiments to explore the potential applications of these compounds are underway, as well as efforts to develop more sensitive copper(II) agents.

4. EXPERIMENTAL SECTION

4.1. Materials and Analysis. All reagents were purchased from Sigma-Aldrich and used without further purification unless stated otherwise. Accurate mass measurements were recorded in a positive electrospray ionization (ESI) mode in CH_3OH or CH_3CN on a Thermo Electron LTQ-Orbitrap Hybrid MS (Thermo Fisher Scientific Waltham, MA). ^1H and ^{13}C NMR spectra were measured in the solvent stated at 400 or 600 MHz and 101 or 151 MHz, respectively (Bruker AVIIIHD Nanobay 400 MHz and Bruker VNMRS 600 MHz, Bruker LLC, Billerica, MA). UV−vis absorption spectra were recorded in a 1.0 cm path length and 700 μL quartz cuvettes on a Cary Bio-100 UV−vis spectrophotometer (Agilent, Santa Clara, CA). All metal salts were prepared in deionized ultrafiltered (D.I.U.F) water purchased from Fisher Scientific.

4.2. Synthesis. *4.2.1. 5-Methoxy-1,2,3,3-tetramethyl-3H-indol-1-ium iodide (1).*[100] Following a modified literature procedure,[101] 4-methoxyphenylhydrazine hydrochloride (4.815 g, 27.57 mmol) was added to a solution containing 3-methylbutan-2-one (5.90 mL, 55.2 mmol) in glacial acetic acid (88 mL). The solution was stirred at reflux for 5.5 h. The solution was allowed to cool to room temperature and neutralized with KOH pellets. The crude material was extracted with Et_2O (3 × 100 mL), dried over $MgSO_4$, filtered, and concentrated in vacuo. The crude product was purified by flash column chromatography (70:30, hexanes/EtOAc) to afford 2,3,3-trimethyl-5-methoxy-3*H*-indole as a red amorphous solid (5.149 g, 99%). ^1H NMR (600 MHz, $CDCl_3$) δ 7.43 (d, J = 8.3 Hz, 1H), 6.84−6.80 (m, 2H), 3.82 (s, 3H), 2.24 (s, 3H), 1.28 (s, 6H). ^1H NMR is consistent with published data.[102] Following a modified literature procedure,[100] iodomethane (0.048 mL, 0.76 mmol) was added to a solution of 2,3,3-trimethyl-5-methoxy-3*H*-indole (0.133 g, 0.716 mmol) in anhydrous acetonitrile (14.3 mL). The solution was stirred at reflux for 21 h. The solution was allowed to cool to room temperature, concentrated in vacuo, and suspended in $CHCl_3$ (2.5 mL) and hexanes (20 mL). The suspension was sonicated for 30 min and filtered to afford indolium **1** as a pink amorphous solid (0.117 g, 49%). ^1H NMR (600 MHz, $CDCl_3$) δ 7.56 (d, J = 8.7 Hz, 1H), 7.07−7.01 (m, 2H), 4.23 (s, 3H), 3.90 (s, 3H), 3.04 (s, 3H), 1.65 (s, 6H). ^1H NMR is consistent with published data.[100] MS, ESI^+: m/z = 204.14 ($M - H^+$).

4.2.2. 5-Dimethylamino-2-hydroxy-benzaldehyde (2).[103] Following the reported literature,[14] EtOH (30 mL) and an aqueous formaldehyde solution (37%, 3.8 mL) were added to a flask containing 2-hydroxy-5-nitrobenzaldehyde (0.160 g, 0.957 mmol) and Pd/C (20 wt %, 0.098 g). **Caution**: Pd/C is pyrophoric and must be handled under appropriate safety protocols. The solution was purged with argon and then H_2. The mixture was then stirred under a balloon of H_2 for 18 h at room temperature. An additional aqueous formaldehyde solution (37%, 2.0 mL) was added and the mixture was again purged with argon and H_2, and then stirred for an additional 24 h under a H_2 balloon. The mixture was filtered through Celite and the filtrate was acidified with 1 M HCl (15 mL) and concentrated in vacuo. The residue was neutralized with saturated aqueous $NaHCO_3$ and extracted with CH_2Cl_2 (3 × 35 mL). The combined organic extracts were dried over Na_2SO_4 concentrated in vacuo. Purification by flash chromatography (8:2, hexanes/EtOAc) afforded aldehyde **2** as a red oil (0.117 g, 74%). ^1H NMR (600 MHz, $CDCl_3$) δ 10.45 (s, 1H), 9.86 (s, 1H), 7.08 (dd, J = 9.0, 3.1 Hz, 1H), 6.91 (d, J = 9.0 Hz, 1H), 6.85 (d, J = 3.0 Hz, 1H), 2.91 (s, 6H). ^1H NMR was consistent with that reported in the literature.[103]

4.2.3. 5′-Methoxy-N,N,1′,3′,3′-pentamethylspiro-[chromene-2,2′-indolin]-6-amine (SP1). Following the reported literature,[88] salicylaldehyde **2** (0.117 g, 0.708 mmol) and Et_3N (0.20 mL, 1.4 mmol) were added to a solution containing indolium **1** (0.223 g, 0.707 mmol) in EtOH (5.0 mL). The solution was refluxed for 4 h before being concentrated in vacuo. Purification by column chromatography (85:15 to 80:20, hexanes/EtOAc) afforded **SP1** as a red amorphous solid (0.118 g, 47%). IR (cm^{-1}) (Figure S4); 2968 (CH_3 asymmetric stretching), 2874 (CH_3 symmetric stretching), 1650 (C═C stretching), 1600 (aromatic ring), 1488 (CH_3 asymmetric bending), 1390 (CH_3 symmetric bending), 1273 and 1251 (C−N stretching), 1217 (C−O stretching), 1183 ($COCH_3$ stretching), 1127 and 1097 (CH out of plane asymmetric stretching), 1031 and 1010 (CH out of plane symmetric stretching), and 956 (O−C−N stretching); ^1H NMR (600 MHz, $CDCl_3$) (Figure S1); δ 6.81 (d, J = 10.1 Hz, 1H), 6.73 (d, J = 2.5 Hz, 1H), 6.71 (dd, J = 8.2, 2.5 Hz, 1H), 6.66 (d, J = 8.8 Hz, 1H), 6.61 (dd, J = 8.8, 2.9 Hz, 1H), 6.51 (d, J = 2.9 Hz, 1H), 6.43 (d, J = 8.2 Hz, 1H), 5.68 (d, J = 10.1 Hz, 1H), 3.80 (s, 3H), 2.86 (s, 6H), 2.60 (s, 3H), 1.11 (s, 3H), 1.17 (s, 3H); ^1H NMR was consistent with our previous literature report.[88] MS, ESI^+: m/z = 351.21 (**SP1**−H^+) (Figure S3).

4.3. Copper Titration Procedures. The absorption spectra were recorded on a Cary Bio-100 UV−vis spectrometer using a quartz cell with a 1.0 cm path length and a volume of 700 μL. For precision and accuracy, all solutions were freshly prepared and experimental conditions were maintained for all assays. Stock solutions of the cations (1.4×10^{-2} M) were prepared in deionized ultrafiltered (D.I.U.F) water and **SP1** (1×10^{-4} M) was prepared in ethanol in the dark. The titration was accomplished by placing 700 μL of an **SP1** stock solution (1.16×10^{-4} M = 100 μM SP in ethanol) directly into the cuvette and adding copper(II) [Cu^{2+}] from a stock (1.4×10^{-3} M in D.I.U.F. water, 200 μM will be 116.6 μL), diluted to a fixed total volume (816.6 μL) for all concentrations, and incubated in the dark for 15 min. The change in absorbance at 418 and 677 nm was plotted against the copper(II) ion concentration.

4.3.1. Response of Phenol and N,N-Dimethylaniline to Cu^{2+} in Ethanol. Absorbance profiles of phenol (100 μM) and *N*,*N*-dimethylaniline (100 μM) were obtained in a 700 μL solution of the above reference compounds after adding varying amounts (0−1.4 equiv) of Cu^{2+} in ethanol and incubating in the dark for 15 min.

4.3.2. Job's Plot Analysis. Data for Job's plot were generated by maintaining fixed total molarity of **SP1** and copper(II) chloride at 1×10^{-4} M while varying the molar equivalents of each. The absorbance was recorded at 677 nm with maximal absorbance achieved at 0.5 molar equivalents of **SP1** and copper(II) chloride. The ratio of copper(II) to **SP1** was systematically varied (0−0.9) keeping fixed total molarity (100 μM) and keeping a constant sample volume (700 μL).

https://doi.org/10.1021/acsomega.1c00392
ACS Omega 2021, 6, 10776−10789

4.3.3. Limit of Detection (LOD). Seven hundred microliters of an **SP1** stock solution (1.02×10^{-4} M = 100 μM SP in ethanol) was added directly into the cuvette. To the cuvette was added a known amount of copper(II) [Cu^{2+}] from a stock (3.8×10^{-5} M in D.I.U.F water, 0.80 μM = 15 μL), diluted to a fixed total volume (715 μL), mixed with a Pasteur pipette, and incubated in the dark for 15 min, followed by absorbance measurement. This was repeated in triplicate for copper(II) concentrations ranging from 0 to 0.80 μM and the triplicates at each concentration were averaged to obtain the value. The order of the copper(II) concentrations was determined using a random number generator. The LOD for the sensor was calculated by first using linear ordinary least-squares (OLS) regression (R version 3.6.0) of baseline-corrected absorbance vs [Cu] in μM to determine the mean square error (MSE). The MSE of OLS was used as an estimate of the error variance σ^2, while the intercept of the OLS fit was taken to be representative of the blank (0 μM) absorbance. The LOD was defined as the minimum [Cu], which resulted in an absorbance no greater than 3σ from the blank.

4.4. Absorbance Profile of SP1 with Equimolar (1×) Metal Chlorides. Seven hundred microliters of a 1×10^{-4} M solution of **SP1** in ethanol was added into a quartz cuvette. This solution, prepared under dark conditions, was scanned for an initial absorbance profile. To the cuvette, 1 equiv of metal chloride was then added (5 μL of a 1.4×10^{-2} M solution of metal chloride in D.I.U.F water) and incubated in the dark for 15 min, followed by absorbance measurement.

4.5. Competition Studies. *4.5.1. Equimolar (1×) Metal Chlorides to Copper(II) Chloride (1×).* Seven hundred microliters of a 1×10^{-4} M solution of **SP1** in ethanol was added into a quartz cuvette. This solution, prepared under dark conditions, was scanned for an initial absorbance profile. To the cuvette, 1 equiv of metal chloride was then added (5 μL of a 1.4×10^{-2} M solution of metal chloride in D.I.U.F water) and 1 equiv of copper(II) chloride (5 μL of a 1.4×10^{-2} M solution of copper(II) chloride in D.I.U.F water), mixed with a Pasteur pipette, incubated under dark for 15 min, followed by absorbance measurement. For the images in Figure 7, these procedures were scaled to 21.4 μL of metal chloride, 21.4 μL of copper(II) chloride, and 3 mL of ethanol (metals only) or 3 mL of **SP1** (colorimetric detection).

4.5.2. Ten Equivalents (10×) Metal Chlorides to Copper(II) Chloride (1×). Seven hundred microliters of a 1×10^{-4} M solution of **SP1** in ethanol was added into a quartz cuvette. This solution, prepared under dark conditions, was scanned for an initial absorbance profile. To the cuvette, 10 equiv of metal chloride was then added (50 μL of a 1.4×10^{-2} M solution of metal chloride in D.I.U.F water), mixed with a Pasteur pipette, incubated under dark for 15 min, followed by absorbance measurement. Subsequently, 1 equiv of copper(II) chloride (5 μL of a 1.4×10^{-2} M solution of copper(II) chloride in D.I.U.F water) was added to the cuvette, mixed with a Pasteur pipette, incubated under dark for 15 min, followed by absorbance measurement. For the images in Figure 7, these procedures were scaled to 214 μL of metal chloride, 21.4 μL of copper(II) chloride, and 3 mL of ethanol (metals only) or 3 mL of **SP1** (colorimetric detection).

4.6. Assessing Sensor Predictive Capacity. To assess the predictive performance of the spiropyran-based Cu^{2+} sensor, a logistic regression (Binomial GLM, logit link) model in R (version 3.6.0) was used. The response was coded as 0-1 with 1 representing the presence of Cu and with a classification cutoff probability of 0.5. The model was initially fitted on the 10× data set (training set) and leave-one-out cross-validation was used to assess the overall accuracy, false-positive rate (FPR), and false-negative rate (FNR) within the 10× training set. Following this, the same model was used to predict the presence of Cu on the 1× data set (test set). Model performance was again assessed through overall accuracy, FPR, and FNR on the 1× test set.

4.7. Computational Analysis. Calculations were carried out for the following complexes: SP1−Cu^{2+}, SP1−Fe^{3+}, SP1−Ca^{2+}, and SP1−Na^{+}. The metal ions were chosen to have representations from the transition, alkali, and alkaline-earth metals and to have different magnitudes of positive charges. Density functional theory (DFT)[104] calculations were performed to determine the equilibrium structures using the PBE0[105] functional and 6-31+G(d,p) as the basis set for the C, O, H, and N atoms, while the LANL2DZ pseudopotential was used for Cu^{2+} (DFT/PBE0/6-31+G(d,p)-LANL2DZ). The solvent effects were considered by applying the polarizable continuum model (PCM)[106] with ethanol as the solvent in all calculations. All equilibrium geometries were then subjected to frequency analysis to confirm that they all correspond to true minima. The total energies were then calculated using the DFT/PBE0/6-31+G(d,p)-LANL2DZ method, while the excited states were simulated using the TD- DFT/PBE0/6-31+G(d,p)-LANL2DZ. For the other metals tested, Ca^{2+} and Na^{+} used the 6-31+G basis, while Fe^{3+} used the LANL2DZ pseudopotential at the same level of theory. NBO population analysis was carried out using the NBO 7.0 program.[107] Chemical structures were viewed using GaussView 6[108] and Chemcraft.[109] The UV−vis analysis was done using the GaussSum package.[110]

■ ASSOCIATED CONTENT

Supporting Information

The Supporting Information is available free of charge at https://pubs.acs.org/doi/10.1021/acsomega.1c00392.

NMR spectra (^{1}H and ^{13}C), ESI-MS, IR, and the optimized structure of SP1; the simulated absorbance spectrum, experimental UV−vis absorbance spectrum, optimized structure, Job's plot values, additional data from 10× competition studies, and analysis with copper nitrate and copper perchlorate for the SP1−Cu^{2+} complex; the absorbance profile of copper chloride, metal chlorides (1×), and metal chlorides (10×) in ethanol; and HOMO−LUMO gaps of SP1−Cu^{2+}, SP1−Fe^{3+}, SP1−Ca^{2+}, and SP1−Na^{+} complexes (PDF)

■ AUTHOR INFORMATION

Corresponding Authors

Joel Garcia − *Department of Biomedical Engineering, University of California at Davis, Davis, California 95616, United States; Chemistry Department, De La Salle University, 1004 Manila, Philippines*; Email: joel.garcia@dlsu.edu.ph

Angelique Y. Louie − *Chemistry Graduate Group, University of California at Davis, Davis, California 95616, United States; Department of Biomedical Engineering, University of California at Davis, Davis, California 95616, United States;* orcid.org/0000-0001-6610-5356; Email: aylouie@ucdavis.edu

https://doi.org/10.1021/acsomega.1c00392
ACS Omega 2021, 6, 10776−10789

Authors

Kimberly M. Trevino − *Chemistry Graduate Group, University of California at Davis, Davis, California 95616, United States;* orcid.org/0000-0001-5286-4861

Brandon K. Tautges − *Chemistry Graduate Group, University of California at Davis, Davis, California 95616, United States*

Rohan Kapre − *Department of Biomedical Engineering, University of California at Davis, Davis, California 95616, United States*

Francisco C. Franco Jr − *Chemistry Department, De La Salle University, 1004 Manila, Philippines;* orcid.org/0000-0002-8339-2411

Victor W. Or − *Department of Biomedical Engineering, University of California at Davis, Davis, California 95616, United States*

Edward I. Balmond − *Chemistry Graduate Group, University of California at Davis, Davis, California 95616, United States;* orcid.org/0000-0002-9726-4488

Jared T. Shaw − *Chemistry Graduate Group, University of California at Davis, Davis, California 95616, United States;* orcid.org/0000-0001-5190-493X

Complete contact information is available at: https://pubs.acs.org/10.1021/acsomega.1c00392

Author Contributions

All authors have given approval to the final version of the manuscript.

Notes

The authors declare no competing financial interest.

■ ACKNOWLEDGMENTS

The authors thank the Keck Foundation for support of this work. The authors would also like to thank DOST-PCIEERD for the computational resources.

■ REFERENCES

(1) Zhu, H.; Fan, J.; Wang, B.; Peng, X. Fluorescent, MRI, and Colorimetric Chemical Sensors for the First-Row d-Block Metal Ions. *Chem. Soc. Rev.* **2015**, *44*, 4337−4366.

(2) Carter, K. P.; Young, A. M.; Palmer, A. E. Fluorescent Sensors for Measuring Metal Ions in Living Systems. *Chem. Rev.* **2014**, *114*, 4564−4601.

(3) Thompson, K. H.; Orvig, C. Boon and Bane of Metal Ions in Medicine. *Science* **2003**, *300*, 936−939.

(4) Verwilst, P.; Sunwoo, K.; Kim, J. S. The Role of Copper Ions in Pathophysiology and Fluorescent Sensors for the Detection Thereof. *Chem. Commun.* **2015**, *51*, 5556−5571.

(5) Danks, D. M. The Metabolic Basis of Inherited Disease. 6th Edition. *Jpn. J. Hum. Genet.* **1989**, *34*, 253.

(6) Harris, E. D. Copper Transport: An Overview. *Exp. Biol. Med.* **1991**, *196*, 130−140.

(7) Tiffany-Castiglioni, E.; Qian, Y. Astroglia as Metal Depots: Molecular Mechanisms for Metal Accumulation, Storage and Release. *Neurotoxicology* **2001**, *22*, 577−592.

(8) Brewer, G. J. Copper Excess, Zinc Deficiency, and Cognition Loss in Alzheimer's Disease. *BioFactors* **2012**, *38*, 107−113.

(9) Brewer, G. J. Copper-2 Ingestion, Plus Increased Meat Eating Leading to Increased Copper Absorption, Are Major Factors Behind the Current Epidemic of Alzheimer's Disease. *Nutrients* **2015**, *7*, 10053−10064.

(10) Barnham, K. J.; Bush, A. I. Biological Metals and Metal-Targeting Compounds in Major Neurodegenerative Diseases. *Chem. Soc. Rev.* **2014**, *43*, 6727−6749.

(11) Gaggelli, E.; Kozlowski, H.; Valensin, D.; Valensin, G. Copper Homeostasis and Neurodegenerative Disorders (Alzheimer's, Prion, and Parkinson's Diseases and Amyotrophic Lateral Sclerosis). *Chem. Rev.* **2006**, *106*, 1995−2044.

(12) Pall, H. S.; Blake, D. R.; Gutteridge, J. M.; Williams, A. C.; Lunec, J.; Hall, M.; Taylor, A. Raised Cerebrospinal-Fluid Copper Concentration in Parkinson's Disease. *Lancet* **1987**, *330*, 238−241.

(13) Bull, P. C.; Thomas, G. R.; Rommens, J. M.; Forbes, J. R.; Cox, D. W. The Wilson Disease Gene Is a Putative Copper Transporting P−Type ATPase Similar to the Menkes Gene. *Nat. Genet.* **1993**, *5*, 327−337.

(14) Ahuja, A.; Dev, K.; Tanwar, R. S.; Selwal, K. K.; Tyagi, P. K. Copper Mediated Neurological Disorder: Visions into Amyotrophic Lateral Sclerosis, Alzheimer and Menkes Disease. *J. Trace Elem. Med. Biol.* **2015**, *29*, 11−23.

(15) Valentine, J. S.; Doucette, P. A.; Zittin Potter, S. Copper-Zinc Superoxide Dismutase Amyotrohpic Lateral Sclerosis. *Annu. Rev. Biochem.* **2005**, *74*, 563−593.

(16) Bourassa, M. W.; Brown, H. H.; Borchelt, D. R.; Vogt, S.; Miller, L. M. Metal-Deficient Aggregates and Diminished Copper Found in Cells Expressing SOD1 Mutations That Cause ALS. *Front. Aging Neurosci.* **2014**, *6*, 1−6.

(17) Wuana, R. A.; Okieimen, F. E. Heavy Metals in Contaminated Soils: A Review of Sources, Chemistry, Risks and Best Available Strategies for Remediation. *ISRN Ecol.* **2011**, *2011*, 1−20.

(18) Cassella, R. J.; Brum, D. M.; Lima, C. F.; Fonseca, T. C. O. Direct Determination of Cu and Fe in Jet Fuel by Electrothermal Atomic Absorption Spectrometry with Injection of Sample as Detergent Emulsions. *Fuel* **2011**, *90*, 1215−1220.

(19) Worms, I.; Simon, D. F.; Hassler, C. S.; Wilkinson, K. J. Bioavailability of Trace Metals to Aquatic Microorganisms: Importance of Chemical, Biological and Physical Processes on Bio-uptake. *Biochimie* **2006**, *88*, 1721−1731.

(20) Levy, J. L.; Stauber, J. L.; Jolley, D. F. Sensitivity of Marine Microalgae to Copper: The Effect of Biotic Factors on Copper Adsorption and Toxicity. *Sci. Total Environ.* **2007**, *387*, 141−154.

(21) Meador, J. P. The Interaction of PH, Dissolved Organic Carbon, and Total Copper in the Determination of Ionic Copper and Toxicity. *Aquat. Toxicol.* **1991**, *19*, 13−31.

(22) Winner, R. W.; Farrell, M. P. Acute and Chronic Toxicity of Copper to Four Species of Daphnia. *Can. J. Fish. Aquat.* **1976**, *33*, 1685−1691.

(23) Becker, J. S.; Zoriy, M. V.; Pickhardt, C.; Palomero-Gallagher, N.; Zilles, K. Imaging of Copper, Zinc, and Other Elements in Thin Section of Human Brain Samples (Hippocampus) by Laser Ablation Inductively Coupled Plasma Mass Spectrometry. *Anal. Chem.* **2005**, *77*, 3208−3216.

(24) Stadler, N.; Lindner, R. A.; Davies, M. J. Direct Detection and Quantification of Transition Metal Ions in Human Atherosclerotic Plaques: Evidence for the Presence of Elevated Levels of Iron and Copper. *Arterioscler., Thromb., Vasc. Biol.* **2004**, *24*, 949−954.

(25) Kazi, T. G.; Afridi, H. I.; Kazi, N.; Jamali, M. K.; Arain, M. B.; Jalbani, N.; Kandhro, G. A. Copper, Chromium, Manganese, Iron, Nickel, and Zinc Levels in Biological Samples of Diabetes Mellitus Patients. *Biol. Trace Elem. Res.* **2008**, *122*, 1−18.

(26) Ghaedi, M.; Ahmadi, F.; Shokrollahi, A. Simultaneous Preconcentration and Determination of Copper, Nickel, Cobalt and Lead Ions Content by Flame Atomic Absorption Spectrometry. *J. Hazard. Mater.* **2007**, *142*, 272−278.

(27) Shokrollahi, A.; Ghaedi, M.; Hossaini, O.; Khanjari, N.; Soylak, M. Cloud Point Extraction and Flame Atomic Absorption Spectrometry Combination for Copper(II) Ion in Environmental and Biological Samples. *J. Hazard. Mater.* **2008**, *160*, 435−440.

(28) Kim, K. B.; Kim, H.; Song, E. J.; Kim, S.; Noh, I.; Kim, C. A Cap-Type Schiff Base Acting as a Fluorescence Sensor for Zinc(Ii) and a Colorimetric Sensor for Iron(Ii), Copper(Ii), and Zinc(Ii) in Aqueous Media. *Dalton Trans.* **2013**, *42*, 16569−16577.

(29) Park, G. J.; Hwang, I. H.; Song, E. J.; Kim, H.; Kim, C. A Colorimetric and Fluorescent Sensor for Sequential Detection of Copper Ion and Cyanide. *Tetrahedron* **2014**, *70*, 2822−2828.
(30) Tautges, B.; Or, V.; Garcia, J.; Shaw, J. T.; Louie, A. Y. Preparation of a Conjugation-Ready Thiol Responsive Molecular Switch. *Tetrahedron Lett.* **2015**, *56*, 6569−6573.
(31) Zeng, L.; Miller, E. W.; Pralle, A.; Isacoff, E. Y.; Chang, C. J. A Selective Turn-On Fluorescent Sensor for Imaging Copper in Living Cells. *J. Am. Chem. Soc.* **2006**, *128*, 10−11.
(32) Krämer, R. Fluorescent Chemosensors for Cu2+ions: Fast, Selective, and Highly Sensitive. *Angew. Chem., Int. Ed.* **1998**, 772−773.
(33) Wan, F.; Sun, H.; Fan, S. Design of a Portable UV-Vis Spectrophotometer. *Guangpuxue Yu Guangpu Fenxi* **2006**, *26*, 779−783.
(34) An, R.; Zhang, D.; Chen, Y.; Cui, Y.-z. A "Turn-on" Fluorescent and Colorimetric Sensor for Selective Detection of Cu2+ in Aqueous Media and Living Cells. *Sens. Actuators, B* **2016**, *222*, 48−54.
(35) Zhang, J.; Zhao, B.; Li, C.; Zhu, X.; Qiao, R. A BODIPY-Based "Turn-on" Fluorescent and Colorimetric Sensor for Selective Detection of Cu2+ in Aqueous Media and Its Application in Cell Imaging. *Sens. Actuators, B* **2014**, *196*, 117−122.
(36) Noh, J. Y.; Park, G. J.; Na, Y. J.; Jo, H. Y.; Lee, S. A.; Kim, C. A Colorimetric "Naked-Eye" Cu(Ii) Chemosensor and PH Indicator in 100% Aqueous Solution. *Dalton Trans.* **2014**, *43*, 5652−5656.
(37) Fu, Y.; Fan, C.; Liu, G.; Pu, S. A Colorimetric and Fluorescent Sensor for Cu2+ and F− Based on a Diarylethene with a 1,8-Naphthalimide Schiff Base Unit. *Sens. Actuators, B* **2017**, *239*, 295−303.
(38) You, G. R.; Park, G. J.; Lee, J. J.; Kim, C. A Colorimetric Sensor for the Sequential Detection of Cu2+ and CN- in Fully Aqueous Media: Practical Performance of Cu2+. *Dalton Trans.* **2015**, *44*, 9120−9129.
(39) Liu, Y.; Wang, L.; Guo, C.; Hou, Y. A Colorimetric Squaraine-Based Probe and Test Paper for Rapid Naked Eyes Detection of Copper Ion (II). *Tetrahedron Lett.* **2018**, *59*, 3930−3933.
(40) Jo, T. G.; Na, Y. J.; Lee, J. J.; Lee, M. M.; Lee, S. Y.; Kim, C. A Diaminomaleonitrile Based Selective Colorimetric Chemosensor for Copper(Ii) and Fluoride Ions. *New J. Chem.* **2015**, *39*, 2580−2587.
(41) Li, J.; Guo, Y.; Yao, H.; Lin, Q.; Xie, Y.; Wei, T.; Zhang, Y. A Highly Selective Colorimetric Sensor for Cu2+ Based on Phenolic Group Biscarbonyl Hydrazone. *Chin. J. Chem.* **2013**, *31*, 271−276.
(42) Mahapatra, A. K.; Hazra, G.; Das, N. K.; Goswami, S. A Highly Selective Triphenylamine-Based Indolylmethane Derivatives as Colorimetric and Turn-off Fluorimetric Sensor toward Cu2+ Detection by Deprotonation of Secondary Amines. *Sens. Actuators, B* **2011**, *156*, 456−462.
(43) Park, G. J.; You, G. R.; Choi, Y. W.; Kim, C. A Naked-Eye Chemosensor for Simultaneous Detection of Iron and Copper Ions and Its Copper Complex for Colorimetric/Fluorescent Sensing of Cyanide. *Sens. Actuators, B* **2016**, *229*, 257−271.
(44) Gupta, V. K.; Mergu, N.; Kumawat, L. K. A New Multifunctional Rhodamine-Derived Probe for Colorimetric Sensing of Cu(II) and Al(III) and Fluorometric Sensing of Fe(III) in Aqueous Media. *Sens. Actuators, B* **2016**, *223*, 101−113.
(45) Kim, M. S.; Lee, S. Y.; Jung, J. M.; Kim, C. A New Schiff-Base Chemosensor for Selective Detection of Cu2+ and Co2+ and Its Copper Complex for Colorimetric Sensing of S2- in Aqueous Solution. *Photochem. Photobiol. Sci.* **2017**, *16*, 1677−1689.
(46) Li, T.; Yang, Z.; Li, Y.; Liu, Z.; Qi, G.; Wang, B. A Novel Fluorescein Derivative as a Colorimetric Chemosensor for Detecting Copper(II) Ion. *Dyes Pigm.* **2011**, *88*, 103−108.
(47) Wang, H. H.; Xue, L.; Fang, Z. J.; Li, G. P.; Jiang, H. A Colorimetric and Fluorescent Chemosensor for Copper Ions in Aqueous Media and Its Application in Living Cells. *New J. Chem.* **2010**, *34*, 1239−1242.
(48) Fang, H.; Huang, P. C.; Wu, F. Y. A Novel Jointly Colorimetric and Fluorescent Sensor for Cu2+ Recognition and Its Complex for Sensing S2− by a Cu2+ Displacement Approach in Aqueous Media. *Spectrochim. Acta, Part A* **2018**, *204*, 568−575.
(49) Yeh, J. T.; Chen, W. C.; Liu, S. R.; Wu, S. P. A Coumarin-Based Sensitive and Selective Fluorescent Sensor for Copper(II) Ions. *New J. Chem.* **2014**, *38*, 4434−4439.
(50) Kumar, R.; Jain, H.; Gahlyan, P.; Joshi, A.; Ramachandran, C. N. A Highly Sensitive Pyridine-Dicarbohydrazide Based Chemosensor for Colorimetric Recognition of Cu2+, AMP2-, F- and AcO- Ions. *New J. Chem.* **2018**, *42*, 8567−8576.
(51) Manna, A. K.; Mondal, J.; Rout, K.; Patra, G. K. A Benzohydrazide Based Two-in-One Ni2+/Cu2+ Fluorescent Colorimetric Chemosensor and Its Applications in Real Sample Analysis and Molecular Logic Gate. *Sens. Actuators, B* **2018**, *275*, 350−358.
(52) Gu, Z.; Cheng, H.; Shen, X.; He, T.; Jiang, K.; Qiu, H.; Zhang, Q.; Yin, S. A BODIPY Derivative for Colorimetric Fluorescence Sensing of Hg2+, Pb2+ and Cu2+ Ions and Its Application in Logic Gates. *Spectrochim. Acta, Part A* **2018**, *203*, 315−323.
(53) Tang, X.; Zhu, Z.; Wang, Y.; Han, J.; Ni, L.; Wang, L.; Zhang, H.; Li, J.; Qiu, Y. A Dual Site Controlled Probe for Fluorescent Monitoring of Intracellular PH and Colorimetric Monitoring of Cu2+. *Sens. Actuators, B* **2018**, *270*, 35−44.
(54) Liu, M. X.; Wei, T. B.; Lin, Q.; Zhang, Y. M. A Novel 5-Mercapto Triazole Schiff Base as a Selective Chromogenic Chemosensor for Cu 2+. *Spectrochim. Acta, Part A* **2011**, *79*, 1837−1842.
(55) Mohammadi, A.; Khalili, B.; Haghayegh, A. S. A Novel Chromone Based Colorimetric Sensor for Highly Selective Detection of Copper Ions: Synthesis, Optical Properties and DFT Calculations. *Spectrochim. Acta, Part A* **2019**, *222*, 117193/1−117193/8.
(56) Xie, P.; Zhu, Y.; Huang, X.; Gao, G.; Wei, F.; Guo, F.; Jiang, S.; Wang, C. A Novel Probe Based on Rhodamine 101 Spirolactam and 2-(2′-Hydroxy-5′-Methylphenyl)Benzothiazole Moieties for Three-in-One Detection of Paramagnetic Cu2+, Co2+ and Ni2+. *Spectrochim. Acta, Part A* **2019**, *222*, 117171/1−117171/8.
(57) Liu, A.; Yang, L.; Zhang, Z.; Zhang, Z.; Xu, D. A Novel Rhodamine-Based Colorimetric and Fluorescent Sensor for the Dual-Channel Detection of Cu2+ and Fe3+ in Aqueous Solutions. *Dyes Pigm.* **2013**, *99*, 472−479.
(58) Sharma, P.; Singh, P. A Perylene Diimide-Based near-IR Ratiometric Sensor for Detection of Cu2+ Ions: Ensemble for Discrimination of CN- and S2- Ions. *Anal. Methods* **2020**, *12*, 758−767.
(59) Gu, B.; Huang, L.; Xu, Z.; Tan, Z.; Meng, H.; Yang, Z.; Chen, Y.; Peng, C.; Xiao, W.; Yu, D.; Li, H. A Reaction-Based, Colorimetric and near-Infrared Fluorescent Probe for Cu2+ and Its Applications. *Sens. Actuators, B* **2018**, *273*, 118−125.
(60) Tang, L.; Dai, X.; Wen, X.; Wu, D.; Zhang, Q. A Rhodamine-Benzothiazole Conjugated Sensor for Colorimetric, Ratiometric and Sequential Recognition of Copper(II) and Sulfide in Aqueous Media. *Spectrochim. Acta, Part A* **2015**, *139*, 329−334.
(61) Peralta-Domínguez, D.; Rodriguez, M.; Ramos-Ortiz, G.; Maldonado, J. L.; Luna-Moreno, D.; Ortiz-Gutierrez, M.; Barba, V. A Schiff Base Derivative Used as Sensor of Copper through Colorimetric and Surface Plasmon Resonance Techniques. *Sens. Actuators, B* **2016**, *225*, 221−227.
(62) Liu, Y. W.; Chir, J. L.; Wang, S. T.; Wu, A. T. A Selective Colorimetric Sensor for Cu2+ in Aqueous Solution. *Inorg. Chem. Commun.* **2014**, *45*, 112−115.
(63) Kim, H.; Na, Y. J.; Song, E. J.; Kim, K. B.; Bae, J. M.; Kim, C. A Single Colorimetric Sensor for Multiple Target Ions: The Simultaneous Detection of Fe2+ and Cu2+ in Aqueous Media. *RSC Adv.* **2014**, *4*, 22463−22469.
(64) Jung, J. Y.; Kang, M.; Chun, J.; Lee, J.; Kim, J.; Kim, J.; Kim, Y.; Kim, S. J.; Lee, C.; Yoon, J. A Thiazolothiazole Based Cu2+ Selective Colorimetric and Fluorescent Sensor via Unique Radical Formation. *Chem. Commun.* **2013**, *49*, 176−178.
(65) Patil, S. R.; Nandre, J. P.; Patil, P. A.; Sahoo, S. K.; Devi, M.; Pradeep, C. P.; Fabiao, Y.; Chen, L.; Redshaw, C.; Patil, U. D. A Uracil Nitroso Amine Based Colorimetric Sensor for the Detection of Cu2+ Ions from Aqueous Environment and Its Practical Applications. *RSC Adv.* **2015**, *5*, 21464−21470.

https://doi.org/10.1021/acsomega.1c00392
ACS Omega 2021, 6, 10776−10789

(66) Narayanaswamy, N.; Govindaraju, T. Aldazine-Based Colorimetric Sensors for Cu2+ and Fe 3+. *Sens. Actuators, B* **2012**, *161*, 304−310.
(67) Samanta, S.; Manna, U.; Ray, T.; Das, G. An Aggregation-Induced Emission (AIE) Active Probe for Multiple Targets: A Fluorescent Sensor for Zn2+ and Al3+ & a Colorimetric Sensor for Cu2+ and F-. *Dalton Trans.* **2015**, *44*, 18902−18910.
(68) Hrishikesan, E.; Saravanan, C.; Kannan, P. Bis-Triazole-Appended Azobenzene Chromophore for Selective Sensing of Copper(II) Ion. *Ind. Eng. Chem. Res.* **2011**, *50*, 8225−8229.
(69) Lin, Q.; Chen, P.; Liu, J.; Fu, Y. P.; Zhang, Y. M.; Wei, T. B. Colorimetric Chemosensor and Test Kit for Detection Copper(II) Cations in Aqueous Solution with Specific Selectivity and High Sensitivity. *Dyes Pigm.* **2013**, *98*, 100−105.
(70) Aydin, Z.; Keles, M. Colorimetric Detection of Copper(II) Ions Using Schiff-Base Derivatives. *ChemistrySelect* **2020**, *5*, 7375−7381.
(71) Chang, I. J.; Choi, M. G.; Jeong, Y. A.; Lee, S. H.; Chang, S. K. Colorimetric Determination of Cu2+ in Simulated Wastewater Using Naphthalimide-Based Schiff Base. *Tetrahedron Lett.* **2017**, *58*, 474−477.
(72) Gao, Q.; Ji, L.; Wang, Q.; Yin, K.; Li, J.; Chen, L. Colorimetric Sensor for Highly Sensitive and Selective Detection of Copper Ion. *Anal. Methods* **2017**, *9*, 5094−5100.
(73) Abebe, F. A.; Sinn, E. Fluorescein-Based Fluorescent and Colorimetric Chemosensors for Copper in Aqueous Media. *Tetrahedron Lett.* **2011**, *52*, 5234−5237.
(74) Madhupriya, S.; Elango, K. P. Highly Selective Colorimetric Sensing of Cu(II) Ions in Aqueous Solution via Modulation of Intramolecular Charge Transfer Transition of Aminonaphthoquinone Chemosensor. *Spectrochim. Acta, Part A* **2012**, *97*, 100−104.
(75) Dolai, B.; Bhaumik, A.; Pramanik, N.; Ghosh, K. S.; Atta, A. K. Naphthaldimine-Based Simple Glucose Derivative as a Highly Selective Sensor for Colorimetric Detection of Cu2+ Ion in Aqueous Media. *J. Mol. Struct.* **2018**, *1164*, 370−377.
(76) Zhou, H.; Wang, J.; Chen, Y.; Xi, W.; Zheng, Z.; Xu, D.; Cao, Y.; Liu, G.; Zhu, W.; Wu, J.; Tian, Y. New Diaminomaleonitrile Derivatives Containing Aza-Crown Ether: Selective, Sensitive and Colorimetric Chemosensors for Cu(II). *Dyes Pigm.* **2013**, *98*, 1−10.
(77) Kumar, J.; Bhattacharyya, P. K.; Das, D. K. New Duel Fluorescent "on-off" and Colorimetric Sensor for Copper(II): Copper(II) Binds through N Coordination and Pi Cation Interaction to Sensor. *Sens. Actuators, A* **2015**, *138*, 99−104.
(78) Lee, H. Y.; Swamy, K. M. K.; Jung, J. Y.; Kim, G.; Yoon, J. Rhodamine Hydrazone Derivatives Based Selective Fluorescent and Colorimetric Chemodosimeters for Hg2+ and Selective Colorimetric Chemosensor for Cu2. *Sens. Actuators, B* **2013**, *182*, 530−537.
(79) Kaur, P.; Sareen, D.; Singh, K. Selective Colorimetric Sensing of Cu2+ Using Triazolyl Monoazo Derivative. *Talanta* **2011**, *83*, 1695−1700.
(80) Kim, I.; Jeong, D. C.; Lee, M.; Khaleel, Z. H.; Satheeshkumar, C.; Song, C. Triazole-Conjugated Spiropyran: Synthesis, Selectivity toward Cu(II), and Binding Study. *Tetrahedron Lett.* **2015**, *56*, 6080−6084.
(81) Shao, N.; Jian, Y. J.; Wang, H.; Zhang, Y.; Rong, H. Y.; Wing, H. C. Tunable Photochromism of Spirobenzopyran via Selective Metal Ion Coordination: An Efficient Visual and Ratioing Fluorescent Probe for Divalent Copper Ion. *Anal. Chem.* **2008**, *80*, 3466−3475.
(82) Shiraishi, Y.; Tanaka, K.; Hirai, T. Colorimetric Sensing of Cu(II) in Aqueous Media with a Spiropyran Derivative via a Oxidative Dehydrogenation Mechanism. *ACS Appl. Mater. Interfaces* **2013**, *5*, 3456−3463.
(83) Wang, Y.; Xu, Z.; Dai, X.; Li, H.; Yu, S.; Meng, W. A New Spiropyran-Based Sensor for Colorimetric and Fluorescent Detection of Divalent Cu2+ and Hg2+ Ions and Trivalent Ce3+, Cr3+ and Al3+ Ions. *J. Fluoresc.* **2019**, *29*, 569−575.
(84) Xue, Y.; Gong, P.; Tian, J. Specific Recognition of Cu2+ by Simple Spiropyran via Forming a Ternary Complex of Spiropyran-Cu2+-DMF. *Colloids Surf., A* **2018**, *541*, 165−174.
(85) Kumar, A.; Kumar, S. A Benzothiazolinic Spiropyran for Highly Selective, Sensitive and Visible Light Controlled Detection of Copper Ions in Aqueous Solution. *J. Photochem. Photobiol., A* **2020**, *390*, No. 112265.
(86) Kumbhar, H. S.; Gadilohar, B. L.; Shankarling, G. S. A Highly Selective Quinaldine−Indole Based Spiropyran with Intramolecular H-Bonding for Visual Detection of Cu(II) Ions. *Sens. Actuators, B* **2016**, *222*, 35−42.
(87) Guo, Z.-Q.; Chen, W.-Q.; Duan, X.-M. Highly Selective Visual Detection of Cu(II) Utilizing Intramolecular Hydrogen Bond-Stabilized Merocyanine in Aqueous Buffer Solution. *Org. Lett.* **2010**, *12*, 2202−2205.
(88) Balmond, E. I.; Tautges, B. K.; Faulkner, A. L.; Or, V. W.; Hodur, B. M.; Shaw, J. T.; Louie, A. Y. Comparative Evaluation of Substituent Effect on the Photochromic Properties of Spiropyrans and Spirooxazines. *J. Org. Chem.* **2016**, *81*, 8744−8758.
(89) Shao, N.; Zhang, Y.; Cheung, S.; Yang, R.; Chan, W.; Mo, T.; Li, K.; Liu, F. Copper Ion-Selective Fluorescent Sensor Based on the Inner Filter Effect Using a Spiropyran Derivative. *Anal. Chem.* **2005**, *77*, 7294−7303.
(90) Natali, M.; Soldi, L.; Giordani, S. A Photoswitchable Zn (II) Selective Spiropyran-Based Sensor. *Tetrahedron* **2010**, *66*, 7612−7617.
(91) Natali, M.; Giordani, S. Interaction Studies between Photochromic Spiropyrans and Transition Metal Cations: The Curious Case of Copper. *Org. Biomol. Chem.* **2012**, *10*, 1162−1171.
(92) Ford, E. S. Serum Copper Concentration and Coronary Heart Disease among US Adults. *Am. J. Epidemiol.* **2000**, *151*, 1182−1188.
(93) Pieper, K. J.; Martin, R.; Tang, M.; Walters, L.; Parks, J.; Roy, S.; Devine, C.; Edwards, M. A. Evaluating Water Lead Levels During the Flint Water Crisis. *Environ. Sci. Technol.* **2018**, *52*, 8124−8132.
(94) Singha, D.; Das, T.; Satyanarayana, L.; Roy, P.; Nandi, M. Rhodamine Functionalized Mesoporous Silica as a Chemosensor for the Efficient Sensing of Al3+, Cr3+ and Fe3+ Ions and Their Removal from Aqueous Media. *New J. Chem.* **2019**, *43*, 15563−15574.
(95) Kim, H. N.; Ren, W. X.; Kim, J. S.; Yoon, J. Fluorescent and Colorimetric Sensors for Detection of Lead, Cadmium, and Mercury Ions. *Chem. Soc. Rev.* **2012**, 3210−3244.
(96) Zabell, S. L. The Rule of Succession. *Erkenntnis* **1989**, *31*, 283−321.
(97) Frisch, M. J.; Trucks, G. W.; Schlegel, H. B.; Scuseria, G. E.; Robb, M. A.; Cheeseman, J. R.; Scalmani, G.; Barone, V.; Petersson, G. A.; Nakatsuji, H.; Li, X.; Caricato, M.; Marenich, Av.; Bloino, J.; Janesko, B. G.; Gomperts, R.; Mennucci, B.; Hratchian, H. P.; Ortiz, Jv.; Izmaylov, A. F.; Sonnenberg, J. L.; Williams-Young, D.; Ding, F.; Lipparini, F.; Egidi, F.; Goings, J.; Peng, B.; Petrone, A.; Henderson, T.; Ranasinghe, D.; Zakrzewski, V. G.; Gao, J.; Rega, N.; Zheng, G.; Liang, W.; Hada, M.; Ehara, M.; Toyota, K.; Fukuda, R.; Hasegawa, J.; Ishida, M.; Nakajima, T.; Honda, Y.; Kitao, O.; Nakai, H.; Vreven, T.; Throssell, K.; Montgomery, J. A., Jr.; Peralta, J. E.; Ogliaro, F.; Bearpark, M. J.; Heyd, J. J.; Brothers, E. N.; Kudin, K. N.; Staroverov, V. N.; Keith, T. A.; Kobayashi, R.; Normand, J.; Raghavachari, K.; Rendell, A. P.; Burant, J. C.; Iyengar, S. S.; Tomasi, J.; Cossi, M.; Millam, J. M.; Klene, M.; Adamo, C.; Cammi, R.; Ochterski, J. W.; Martin, R. L.; Morokuma, K.; Farkas, O.; Foresman, J. B.; Fox, D. J.. *Gaussian 16*, revision C.01; Gaussian, Inc.: Wallingford, CT, 2016.
(98) Franco, F. C.; Padama, A. A. B. On the Structural and Optoelectronic Properties of Chemically Modified Oligothiophenes with Electron-Withdrawing Substituents for Organic Solar Cell Applications: A DFT=TDDFT Study. *J. Phys. Soc. Jpn.* **2017**, *86*, 064802/1−064802/8.
(99) Heng, S.; Reineck, P.; Vidanapathirana, A. K.; Pullen, B. J.; Drumm, D. W.; Ritter, L. J.; Schwarz, N.; Bonder, C. S.; Psaltis, P. J.; Thompson, J. G.; Gibson, B. C.; Nicholls, S. J.; Abell, A. D. Rationally Designed Probe for Reversible Sensing of Zinc and Application in Cells. *ACS Omega* **2017**, *2*, 6201−6210.
(100) Bryan Jones, J.; Dodds, D. R. Enzymes in Organic Synthesis. 37.' Preparation and Characterization of Potential Decalindione

https://doi.org/10.1021/acsomega.1c00392
ACS Omega 2021, 6, 10776−10789

Substrates of Horse Liver Alcohol Dehydrogenase. *Can. J. Chem.* **1987**, *65*, 2397−2404.
(101) Tatay, S.; Haque, S. A.; O'Regan, B.; Durrant, J. R.; Verhees, W. J. H.; Kroon, J. M.; Vidal-Ferran, A.; Gaviña, P.; Palomares, E. Kinetic Competition in Liquid Electrolyte and Solid-State Cyanine Dye Sensitized Solar Cells. *J. Mater. Chem.* **2007**, *17*, 3037−3044.
(102) Potisek, S. L.; Davis, D. A.; Sottos, N. R.; White, S. R.; Moore, J. S. Mechanophore-Linked Addition Polymers. *J. Am. Chem. Soc.* **2007**, *129*, 13808−13809.
(103) de Almeida, M. V.; Figueiredo, R. M.; dos Santos, H. F.; da Silva, A. D.; de Almeida, W. B. Synthesis and Theoretical Study of Azido and Amino Inositol Derivatives from L-Quebrachitol. *Tetrahedron Lett.* **2001**, *42*, 2767−2769.
(104) Kohn, W.; Sham, L. J. Self-Consistent Equations Including Exchange and Correlation Effects. *Phys. Rev.* **1965**, *140*, A1133−A1138.
(105) Adamo, C.; Barone, V. Toward Reliable Density Functional Methods without Adjustable Parameters: The PBE0 Model. *J. Chem. Phys.* **1999**, *110*, 6158−6170.
(106) Cossi, M.; Scalmani, G.; Rega, N.; Barone, V. New Developments in the Polarizable Continuum Model for Quantum Mechanical and Classical Calculations on Molecules in Solution. *J. Chem. Phys.* **2002**, *117*, 43−54.
(107) Glendening, E. D.; Landis, C. R.; Weinhold, F. NBO 6.0: Natural Bond Orbital Analysis Program. *J. Comput. Chem.* **2013**, *34*, 1429−1437.
(108) Dennington, R.; Keith, T. A.; Millam, J. M. *GaussView, Version 6.1*; Semichem Inc.: Shawnee Mission, KS, 2016.
(109) *Chemcraft—Graphical Software for Visualization of Quantum Chemistry Computations*. https://www.chemcraftprog.com.
(110) O'boyle, N. M.; Tenderholt, A. L.; Langner, K. M. Cclib: A Library for Package-Independent Computational Chemistry Algorithms. *J. Comput. Chem.* **2008**, *29*, 839−845.

https://doi.org/10.1021/acsomega.1c00392
ACS Omega 2021, 6, 10776−10789